Research on Adaptive Feature Band Extraction Technology Based on Fractional Order Differentiation and Machine Learning

Fang Liu[1], Fei Liu[1], Xian Guo[1], Yikang Ren[1]

[1.] Beijing University of Civil Engineering and Architecture, Beijing, China, 100044

Keywords: Mural salinity damage; Fractional order differentiation; Correlation coefficient; Feature extraction; Machine learning.

Abstract

The Dunhuang murals face severe salt-induced deterioration, yet traditional salinity detection methods are often invasive and inefficient. Hyperspectral remote sensing offers a non-destructive alternative, but current inversion models lack sufficient accuracy. This study proposes a multi-level optimization framework integrating Fractional Order Differentiation (FOD), correlation analysis, and various feature selection strategies alongside Partial Least Squares Regression (PLSR) to develop a robust salinity inversion model. Experimental results demonstrate that the prediction model jointly optimized using FOD spectral transformation and LASSO feature selection achieves a cross-validated coefficient of determination (R^2) of 0.908. This represents a 15.96% improvement in accuracy compared to models relying solely on FOD-transformed spectra. The findings confirm that FOD significantly enhances subtle spectral responses associated with salinity features in hyperspectral data. Furthermore, the LASSO algorithm improves model generalizability through its sparse feature selection mechanism. Collectively, combining FOD spectral transformation with judicious feature selection substantially enhances the precision and reliability of salt damage detection. This approach provides a scientific, efficient, and non-destructive technological foundation for mural preservation and restoration.

1. Introduction

As a prominent cultural heritage site along the Silk Road, the Dunhuang murals possess profound historical, artistic, and scientific significance. Yet, throughout their preservation spanning over 1,600 years, these murals have been persistently threatened by salt-induced weathering (Wang et al., 2023). At the macro level, salt-related deterioration—such as detachment, flaking, and alkali-induced disintegration — constitutes the primary mode of degradation in mural paintings located in arid regions. These processes are closely linked to the regional climate and hydrogeological conditions (Ren and Liu, 2024a). Studies have shown that murals, as porous media, are highly susceptible to capillary action through which groundwater or surface water transports soluble salts (e.g., chlorides, sulfates, and phosphates) to the Mural Plaster layer and its surface. These salts undergo cycles of dissolution and crystallization driven by diurnal fluctuations in temperature and humidity, generating crystallization pressure that leads to fissures, friability, and eventual loss of the pigment layer (Ren and Liu, 2025). At the microscopic level, scanning electron microscopy has revealed the morphological characteristics and vertical stratification of salt crystals—ranging from needle-like structures to amorphous aggregates—affirming capillary salt transport and crystallization as fundamental mechanisms in mural deterioration (Zhang et al., 2025).

In addressing the dynamic monitoring of salinity, hyperspectral remote sensing offers a compelling advantage due to its continuous, high-resolution narrowband spectral data—typically encompassing reflectance information across 400–2500 nm. This spectral range allows the detection of subtle optical variations characteristic of salt minerals in the visible to near-infrared domain. However, hyperspectral datasets suffer from high dimensionality and significant redundancy. Additionally, the spectral features of salts such as NaCl and Na_2SO_4 are often obscured by interference from mural base pigments, binding media, and environmental noise, complicating the accurate isolation of diagnostic absorption features (Guo et al., 2023). Moreover, the high dimensionality and redundancy of hyperspectral data can result in overly complex and unstable models when applied directly. Thus, the relative merits of various feature band extraction techniques—such as correlation-based LASSO regression, Successive Projections Algorithm (SPA), and Competitive Adaptive Reweighted Sampling (CARS)—must be critically assessed in the context of mural salinity prediction (Li et al., 2024).

Despite the promising prospects of hyperspectral remote sensing for salinity content estimation, significant discrepancies in predictive accuracy persist(Mashimbye et al., 2012). To enhance spectral sensitivity to salinity information, researchers have increasingly adopted mathematical differential transformations to excavate latent features. Techniques involving integer-order differentiation, as employed by Guo et al., Zhong et al., and Hou et al(Zhouqian et al., 2023), enhance raw spectra to isolate sensitive bands in a relatively straightforward and replicable manner. However, these approaches may fail to capture key information when faced with complex, multi-scale, and nonlinear spectral data(Fu et al., 2019). By contrast, Fractional Order Differentiation (FOD) offers tunable differentiation orders, enabling the preservation and amplification of weak spectral variations across broader frequency domains. This flexibility renders FOD particularly adept at capturing nonlinear phenomena and complex physical processes, thereby improving both interpretability and predictive power(Sousa et al., 2019).

In recent years, machine learning and FOD have been extensively applied in spectroscopy, especially in the estimation of soil salinity and organic matter content. Their feasibility has been substantiated through numerous studies. For example, Wang et al(Wang et al., 2018) validated various regression models for soil salinity estimation using hyperspectral, HJ-CCD, and Landsat OLI data. They developed optimal spectral indices—including difference, ratio, and normalized algorithms—and employed a Bootstrap–BP neural network to

https://doi.org/10.5194/isprs-archives-XLIX-B2-2026-859-2026 |

compare model performance across different data sources. Similarly, Chen et al(Chen et al., 2022) used PLSR, support vector machines, random forest, ridge regression, XGBoost, and extreme learning machines to estimate heavy metal concentrations, incorporating pollutant levels and conducting thorough statistical validation. Ge et al(Ge et al., 2022) proposed a strategy combining FOD and decision-level fusion to enhance soil salinity diagnosis, demonstrating that GF-5 imagery is suitable for such applications. FOD notably strengthened the spectral-salinity correlation, identified more diagnostic bands, and improved accuracy while reducing model uncertainty. Jia et al(Jia et al., 2024) utilized Pearson correlation, variable importance in projection (VIP), grey relational analysis, and gradient boosting for variable selection, followed by modeling using AdaBoost, extremely randomized trees, LightGBM, and other algorithms. The optimal model was further interpreted using Shapley Additive Explanations (SHAP). Song et al(Song et al., 2023) developed a superior PLSR model using FOD-based spectral transformation and improved regression techniques. Ren et al(Ren and Liu, 2024b) constructed a salinity inversion model for Mural Plaster conductivity affected by phosphate erosion by integrating FOD, a novel three-band spectral index, and the PLSR algorithm. While these studies convincingly demonstrate the potential of combining machine learning and FOD in predicting salinity and organic matter, their performance variability reveals a common bottleneck: the selection and organization of input features. Variations in spectral resolution and signal-to-noise ratio among hyperspectral platforms can exacerbate overfitting and compromise physical interpretability when all bands are indiscriminately included. Therefore, it is imperative to move beyond algorithmic optimization and address this challenge at the source—through refined spectral compression and targeted feature extraction—laying the groundwork for high-precision and robust inversion models.

The goal of hyperspectral dimensionality reduction in salinity prediction is to compress redundant bands and reduce computational complexity while preserving spectral signatures relevant to salt absorption. The central task is to tackle issues stemming from the high dimensionality and redundancy of hyperspectral data. Hence, selecting appropriate spectral features becomes critical for improving model performance and computational efficiency(Ren and Liu, 2024c). A key research challenge has been to identify the most salt-sensitive and physically interpretable bands from among hundreds or even thousands of candidates. Traditional approaches often apply Pearson or partial correlation analysis, removing irrelevant bands based on significance thresholds (e.g., $p < 0.01$)(Ren and Liu, 2024a). Yet, even under strict significance constraints, the resulting feature set typically contains substantial multicollinearity and redundant information. Furthermore, univariate tests fail to account for multivariate interactions and nonlinear effects. Thus, a pressing scientific issue is how to further compress redundancy and emphasize salt-sensitive features following preliminary significance screening, in order to enhance the predictive accuracy of hyperspectral salinity inversion models.

While phosphate is less frequently studied than chlorides or sulfates in mural deterioration, its potential impact on cultural heritage materials has drawn growing attention. Literature on mural conservation(Sansupa et al., 2023) indicates that phosphate accumulation is often linked to microbial activity, conservation materials, or environmental factors such as temperature, humidity, and precipitation. Monitoring phosphate levels thus provides insight into how environmental conditions affect mural preservation. Notably, the deterioration of porous Mural Plaster materials in ancient murals is primarily driven by two factors: (1) chemical erosion caused by salt solutions, and (2) the cumulative crystallization–dissolution cycles induced by diurnal fluctuations in temperature and humidity. The latter mechanism is the dominant cause of pore expansion and fracturing in the plaster matrix. Phosphate salts, under specific hydrothermal conditions, may form dodecahydrates, which are especially prone to such crystallization – dissolution processes(Małysiak et al., 2021). This physical property makes phosphate a notable threat to cultural heritage, underscoring the importance of understanding its behavior for the formulation of effective conservation strategies (Figure 1).

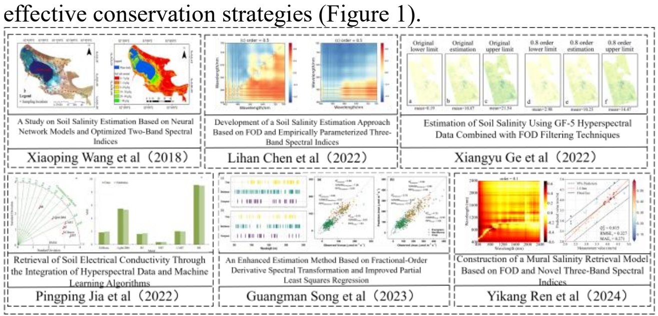

Figure 1 Research Overview.

Improving non-destructive salinity detection in murals and enabling timely early interventions is essential to safeguarding these irreplaceable cultural treasures. Based on in-situ hyperspectral data and synchronous electrical conductivity (EC) measurements from Mural Plaster mock-ups subjected to varying phosphate concentrations, this study aims to:

(1) Evaluate the predictive capacity of coupling data-driven feature selection algorithms with Fractional Order Differentiation (FOD) for mural salinity estimation;

(2) Compare the performance of PLSR models constructed from FOD-transformed spectra under different feature selection strategies;

(3) Identify the optimal PLSR model for phosphate content prediction and elucidate the underlying contribution mechanisms of key spectral bands.

2. Materials and Methodsg

2.1 Study Area and Sample Preparation

Following a comparative analysis of the meteorological conditions in culturally significant heritage sites such as the Yungang Grottoes and the Mogao Caves at Dunhuang, the Mogao Caves were ultimately selected as the study area due to their uniquely extreme climatic conditions, which pose substantial threats to mural preservation. This region exhibits a typical temperate continental climate characterized by scarce precipitation (39.9 mm), intense potential evaporation (≥2486 mm), pronounced annual temperature variability, and strong winds (average speed ≥ 8 m/s on 164 days per year). These extreme thermal fluctuations and significant diurnal temperature differences exert considerable stress on the structural stability of the caves and the integrity of mural materials. The annual mean temperature remains stable at approximately 11.3 ° C, with summer highs reaching 37.6 °C and winter lows plummeting to –20.0 °C. Exterior cave temperatures may occasionally soar to 44 ° C, particularly during July and August, while interior temperatures can drop to as low as –27 °C in November and December. Relative humidity ranges from 27 % to 89 % throughout the year, with an average of 31 % in recent years . These abrupt and cyclical changes in temperature and humidity trigger crystallization–dissolution cycles, promoting continuous salt migration and crystallization processes. These mechanisms are central to pore enlargement and structural disintegration in the Mural Plaster layer. Given that the Mogao Caves not only possess irreplaceable historical and artistic value but also epitomize climatic drivers conducive to salt-induced deterioration, the interplay between meteorological factors and mural degradation emerges as a pivotal focus of this study. Figure 2 illustrates the typical forms of deterioration observed in the murals of the study area.

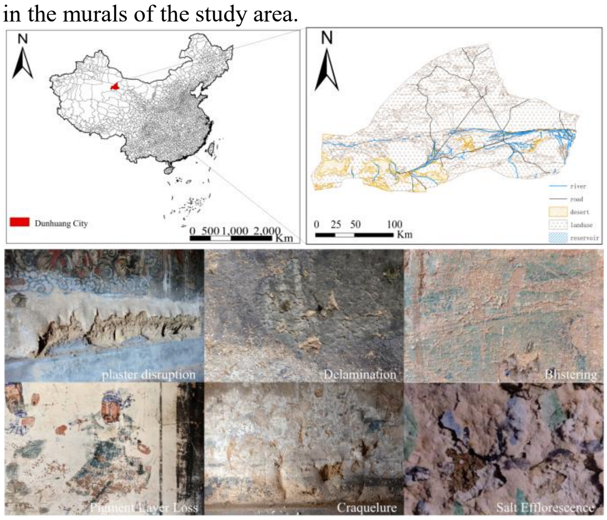

Figure 2 Typical types of mural deterioration in the study area.

The sample preparation protocol was adapted from methods detailed in reference , while the desalination procedure adhered to the standards outlined in GB/T 50123-2019. To eliminate residual salts in the raw materials and thus minimize potential interference with the experimental results, the clay (Chingban soil), sand, and wheat straw underwent a desalination treatment. Specifically, dried soil samples were passed through a 0.56 mm sieve and mixed with deionized water at a 1:5 ratio. The mixture was stirred clockwise for 30 minutes to facilitate salt dissolution, then left undisturbed for 24 hours to allow sedimentation. Once the supernatant had cleared, it was decanted, and this process was repeated five times. The desalination effectiveness was assessed by measuring the electrical conductivity of the soil samples, ensuring that total salt content did not exceed 0.1 %. Post-desalination, the soil was dried, crushed, and sieved for later use. Subsequently, the Mural Plaster mixture was prepared by blending Chingban soil, sand, and wheat straw in a ratio of 64:36:3, followed by the addition of deionized water equivalent to 20 % of the total solid mass. The mixture was thoroughly homogenized and packed into pre-lubricated molds. Surface smoothing and vibration-assisted de-airing were employed to eliminate entrapped air. The molds were then placed in a 90 °C oven to reduce moisture content and approximate a fully dried state, thereby maximizing the authenticity of the samples for simulating actual mural conditions. This comprehensive preprocessing strategy aimed to produce Mural Plaster specimens meeting experimental standards, thereby facilitating subsequent studies on salt-induced degradation.

2.2 Data Acquisition

To investigate the hyperspectral response characteristics of Mural Plaster under varying phosphate concentrations, this study employed five concentrations of disodium hydrogen phosphate dodecahydrate solution: 0.608, 0.808, 1.008, 1.208, and 1.408 mol/L, corresponding to a gradient of salt erosion conditions from mild to severe. Ten replicates were performed for each concentration. Temperature control was maintained at 32.5 °C using a precision low-temperature thermostatic water bath to simulate capillary absorption-driven salt ingress into the plaster samples. This experimental setup was designed to replicate real-world environmental conditions affecting mural salinization as closely as possible. Salt-induced alterations to the surface and internal structure of the Mural Plaster—particularly variations in porosity and surface roughness—are directly correlated with salt damage severity and significantly impact the collection and interpretation of spectral data. The adopted methodology therefore enhances the realism of the simulation and improves the reliability and accuracy of subsequent modeling.

After the samples were air-dried, hyperspectral reflectance measurements were conducted using the ASD FieldSpec 4 Hi-Res spectroradiometer, covering a spectral range from 350 to 2500 nm. To eliminate interference from ambient light, spectral data were acquired in a sealed indoor environment devoid of external illumination. Instrument parameters are detailed in Table 1.

Table 1 Parameters of ASD FieldSpec4 HI-RES Geospectrometer.

Parameter Range	Parameter Values
Spectral Range	350-2500nm
Number of Spectral Channels	2151
Spectral Bandwidth	2.5nm
Spectral Resolution	350-1000nm @ 1.4nm;1001-2500nm @ 2nm
Dimensions	12.7*35.6*29.2cm
Weight	5.44kg

In this experiment, desalination of the raw materials was a crucial step in eliminating confounding variables, thereby ensuring that conductivity measurements could accurately reflect variations induced by phosphate salts rather than other ionic species. Electrical conductivity (EC) served as a key indicator for estimating phosphate concentration in the plaster samples. Based on literature findings, a foundational hypothesis was established: changes in phosphate concentration are closely correlated with shifts in electrical conductivity. Although prior studies have not explicitly linked phosphate levels to EC values, the work of Xiaoguang Zhang, Xiangyu Ge, and others has confirmed that soil solution conductivity can effectively indicate total salinity content. These findings indirectly support the proposed hypothesis by demonstrating EC’s general capacity to reflect salt concentrations in soil matrices. The conductivity measurement procedure involved sieving phosphate-exposed Mural Plaster samples through a 2 mm soil sieve. A soil leachate was prepared using a 1:5 soil-to-water ratio and filtered at a constant room temperature of 25 °C. The EC of the resulting leachate was then determined using a soil salinity EC meter, following protocols described by Ge et al.

https://doi.org/10.5194/isprs-archives-XLIX-B2-2026-859-2026 |

2.3 Hyperspectral Modeling and Experimental Design for Phosphate Content in Mural Plaster

2.3.1 Statistical Analysis and Visualization of Electrical Conductivity Data in Mural Plaster: Descriptive statistical analysis was conducted on the electrical conductivity (EC) data collected from Mural Plaster samples under five distinct experimental conditions. The analysis included assessments of the data’s density distribution, mean, standard deviation (SD), minimum (Min), first quartile (Q1), third quartile (Q3), and coefficient of variation (CV). The coefficient of variation—also referred to as the relative standard deviation—is a standardized measure of dispersion in a probability distribution, defined as the ratio of the standard deviation to the mean. It offers insight into the extent of variability relative to the mean value. A CV $\leqslant$ 15 % is interpreted as indicating low variability; a CV between 15 % and 35 % reflects moderate variability; and a CV > 35 % signifies high variability. The formula for calculating the coefficient of variation is expressed as follows (Equation 1):

$$CV = \frac{\sigma}{u} \times 100\% \tag{1}$$

Where, σ is the sample standard deviation,u is the sample mean.

2.3.2 Preprocessing of Hyperspectral Data: Raw hyperspectral reflectance data inevitably contain noise and spectral spikes, necessitating preprocessing to yield smoother and more interpretable spectral profiles. The goal of preprocessing is to mitigate high-frequency noise, eliminate outliers, and reduce both intrinsic and extrinsic interferences caused by instrument or environmental factors. This step is crucial to ensure the accuracy and reliability of the spectral signal, thereby enhancing the robustness and precision of subsequent quantitative analysis and model construction . Initially, spectral bands with low signal-to-noise ratios—specifically, the 350–399 nm and 2401–2500 nm ranges—were excluded. Subsequently, a Savitzky-Golay filter was applied to the hyperspectral reflectance data from 50 simulated Mural Plaster samples. The filtering employed a polynomial of degree 2 and a window size of 21 data points, offering optimal smoothing performance. The mathematical formulation is presented in Equation 2. During data acquisition, potential sources of surface roughness and cracking were carefully avoided. For each sample, spectral data were collected from five spatially distinct points on the surface, and the average was computed to ensure consistency and minimize localized anomalies.

$$y_i^{'} = \frac{1}{\Delta} \sum_{j=-m}^{m} c_j \cdot y_{i+j} \tag{2}$$

Where, $y_i^{'}$ is the smoothed data point, y_{i+j} is the raw data point in the original sequence, c_j is the convolution coefficients derived via polynomial fitting,m is the half of the window size.

2.3.3 Fractional Order Differentiation: Fractional Order Differentiation (FOD) is a generalization of classical integer-order differentiation and has found wide application in both mathematics and engineering disciplines. Several formulations exist, including Riemann–Liouville (R-L), Riesz, Weyl, Caputo, and Grünwald–Letnikov (G-L) models. In this study, the Grünwald–Letnikov method was adopted due to its discretized formulation, which is particularly well-suited for numerical processing of spectral signals.

2.3.4 Significance Testing: Statistical significance testing was employed to assess whether the observed correlations between spectral features and phosphate concentration were non-random. Specifically, the *p*-value was used as the criterion for evaluating the strength of association (Equations 3 and 4). The Pearson correlation coefficient *r* quantifies the linear relationship between spectral absorption intensity at a given wavelength and phosphate concentration in the Mural Plaster. To assess the significance of the correlation, r was transformed into a *t*-statistic, which accounts for sample size and degrees of freedom (typically $n – 2$, where *n* is the number of data points). The probability of observing such a correlation under the null hypothesis of no association was then calculated using the cumulative distribution function (CDF) of the t-distribution. If the resulting p-value is below a pre-defined significance threshold (e.g., $p < 0.01$), the correlation is deemed statistically significant. This analytical framework supports the conclusion that specific hyperspectral features can serve as reliable indicators for inferring phosphate concentration in Mural Plaster.

$$t = \frac{r\sqrt{n-2}}{\sqrt{1-r^2}} \tag{3}$$

$$\mathrm{p} = 2 \times (1 - \mathrm{CDF}(t, \mathrm{df} = n-2)) \tag{4}$$

where,*n* is the number of observations,r is the Pearson correlation coefficient,*t* is the transformed test statistic, assumed to follow a *t*-distribution under the null hypothesis,CDF(t, df=n-2) is the cumulative distribution function, indicating the probability that the *t*-statistic is less than or equal to the observed value, *p* is the probability metric used to determine statistical significance.

2.4 Feature Selection, Modeling, and Performance Evaluation

2.4.1 Feature Selection: Feature selection is a critical step in hyperspectral data processing. By identifying spectral wavelengths that are highly correlated with the target variable, it enhances both the performance and interpretability of predictive models. In this study, multiple feature selection algorithms were employed, including Least Absolute Shrinkage and Selection Operator (LASSO), Synergy Interval Partial Least Squares (SiPLS), Successive Projections Algorithm (SPA), Competitive Adaptive Reweighted Sampling (CARS), and the Random Frog algorithm. Each method was selected and optimized based on the specific characteristics of hyperspectral data (Table 2 presents the parameter settings for each algorithm). Initially, correlation analysis was conducted to filter out irrelevant wavelengths, retaining only those with statistically significant associations to the target variable in each FOD-processed spectral dataset ($p < 0.01$).

LASSO Regression achieves simultaneous feature sparsification and model fitting via L1-regularization. In this study, the LassoCV algorithm (cross-validated LASSO) was employed to identify non-zero coefficient wavelengths as informative predictors. These wavelengths exhibited the strongest correlation with the response variable. Through cross-validation, the LASSO model adaptively optimized the regularization parameter, mitigating the risk of overfitting. The model was implemented using the scikit-learn library, with a maximum iteration limit set at 10,000.

Synergy Interval Partial Least Squares (SiPLS) is a PLS-based feature selection technique that divides the spectral domain into discrete intervals and evaluates each for predictive relevance. In our study, the full spectral range was partitioned into 10 equal-width sub-intervals, each containing 10 consecutive bands. For each interval, a 2-component PLSR model was constructed, and the predictive performance was assessed using five-fold cross-validation, with negative mean squared error (−MSE) as the evaluation criterion. The most informative intervals were selected for model development. SiPLS effectively reduces multicollinearity among variables and enhances model robustness and predictive precision. The algorithm was implemented via the PLSRegression module in scikit-learn, with a cross-validation step size of 5.

Successive Projections Algorithm (SPA) is an iterative method that identifies wavelengths with the greatest influence on the target variable by maximizing the norm of the projection matrix at each step. The projection matrix was initialized and set as 30 iterations, wavelengths were selected sequentially to maximize the projection vector magnitude, thereby updating the matrix. Custom Python code was used to implement SPA, ultimately retaining 30 wavelength features with the lowest projection residuals.

Competitive Adaptive Reweighted Sampling (CARS) is a sampling-based feature selection algorithm driven by PLS regression. CARS iteratively eliminates low-contribution variables while retaining the most representative spectral features. In each iteration, feature importance was assessed using the absolute values of the PLS regression coefficients. The bottom 10 % of features (with the lowest weights) were pruned until only 10 variables remained. The algorithm, implemented using scikit-learn’s PLSR module, was set to a maximum of 50 iterations, terminating when the number of selected features dropped to 10 or fewer.

Random Frog, a stochastic feature selection technique based on Random Forest regression, estimates feature importance through ensemble learning. In each iteration, 30 % of the spectral features were randomly sampled to construct a Random Forest model (comprising 100 trees, using Gini importance). Importance scores were accumulated across 100 iterations, and the top 20 features with the highest scores were selected. The model was accelerated through parallel computation and implemented using the RandomForestRegressor in scikit-learn.

Table 2 provides a summary of the parameter configurations for each feature selection algorithm.

Methodology	Key Parameters	Toolkit	Number of Output Features
LASSO	Automatic Optimization of λ， max_iter=10,000	scikit-learn	Non-zero Coefficients
SiPLS	Number of Intervals = 10 Number of Cross-Validation Folds = 5	scikit-learn	10
SPA	Maximum Number of Iterations = 30	Custom Implementation	30
CARS	Elimination Rate = 10% Termination Feature Count = 10	scikit-learn	10
Random Frog	Number of Iterations = 100 Subset Ratio = 30%	scikit-learn	20

2.4.2 Partial Least Squares Regression Modeling and Performance Evaluation: To develop a data-driven model for predicting phosphate content in Mural Plaster, the spectral features selected using the methods described in Section 2.4.1 were employed as explanatory variables in Partial Least Squares Regression (PLSR) models. Modeling was conducted separately for each FOD-transformed spectral dataset.

For each method, the selected spectral bands (explanatory variables) were paired with their corresponding electrical conductivity values (response variable) to construct a PLSR model. Using Equations (5) and (6), significant wavelengths identified via correlation testing were integrated into the model as predictors of mural plaster salinity.

Fifty hyperspectral datasets were obtained from Mural Plaster samples exposed to varying levels of saline erosion. These datasets underwent fractional order differentiation (FOD) processing with orders ranging from 0.1 to 2.0. Correlation coefficients were then calculated between the raw and FOD-transformed spectral data and the measured electrical conductivity. Wavelengths exhibiting statistically significant correlations ($p < 0.01$) were retained.

Subsequently, these wavelengths served as inputs for the PLSR model, with electrical conductivity as the dependent variable. Prior to modeling, the data were standardized and mean-centered to improve model precision. The model was constructed using the Kernel PLS algorithm, with the number of latent components capped at seven. The optimal number of components was determined via randomized cross-validation. To ensure model stability and robustness, several diagnostic criteria were applied: thresholds for the calibration-to-validation residual variance ratio were set at 0.5 and 0.75, respectively, while the maximum allowable increase in residual variance was limited to 6 %.

The PLSR modeling process is summarized as follows:

$$X = T \times P^T + E \tag{5}$$

$$Y = U \times Q^T + F \tag{6}$$

Where, X represents the matrix of spectrally significant bands, i.e., the matrix of explanatory variables; Y denotes the electrical conductivity of Mural Plaster, the matrix of response variables. T and U are the score matrices for explanatory and response variables, respectively, while P and Q represent the loading matrices for these variables. E and F are the residual matrices, signifying the aspects of the model that remain unexplained.

2.4.3 Model Accuracy Evaluation Metrics: To evaluate the predictive performance of the developed models, five standard accuracy metrics were employed, including the coefficient of determination (R²), root mean square error (RMSE), and mean absolute error (MAE). The formulas for these indicators are presented in Equations (7)–(9).

$$R^2 = \left(\frac{\sum_{i=1}^{n} \left(y_i - \bar{y}\right)\left(z_i - \bar{z}\right)}{\sqrt{\sum_{i=1}^{n} \left(y_i - \bar{y}\right)^2 \cdot \sum_{i=1}^{n} \left(z_i - \bar{z}\right)^2}} \right)^2 \tag{7}$$

$$RMSE = \sqrt{\frac{\sum_{i=1}^{n} \left(y_i - z_i\right)^2}{n}} \tag{8}$$

$$MAE = \frac{1}{n} \sum_{i=1}^{n} \left| y_i - \hat{y}_i \right| \tag{9}$$

where, n represents the number of mural plaster samples; y_i Represents the EC measurement value of the i^{th} mural plaster sample; $\bar{y}$ Represents the average of the measured values of all mural plaster samples; $\hat{y}_i$ represents the predicted value for the i^{th} sample of Mural Plaster. z_i Represents the predicted EC value of the i^{th} mural plaster sample; $\overline{z}$ Represents the average EC predicted value of all mural floor samples. The performance metrics of the model encompass the coefficient of determination for the calibration dataset, denoted by R_c^2 ,the coefficient of determination for the validation dataset, represented by $RMSE_c$, the coefficient of determination of the validation data set is expressed as R_v^2, the root mean square error for the validation dataset, articulated as $RMSE_v$,and the mean absolute error, delineated as *MAE*.Among them, R^2 is used to evaluate the model fitting degree.The closer the value is to 1, the higher the model accuracy. RMSE and MAE are used to evaluate the stability of the model. The closer the value is to 0, the better the RMSE and MAE are. The workflow is illustrated in Figure 3.

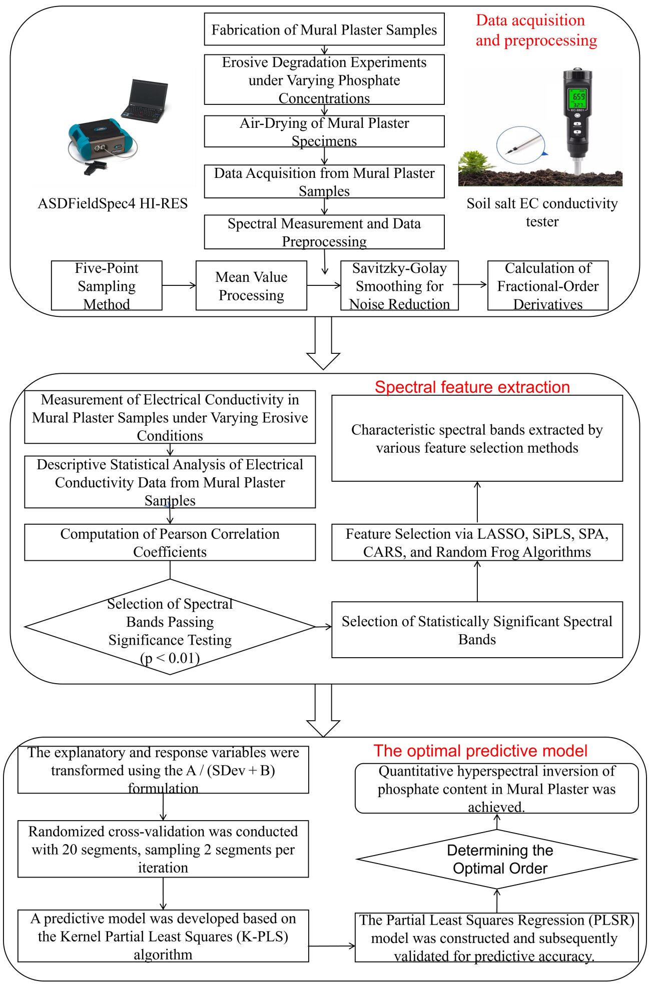

Figure 3 illustrates the overall technical workflow of FOD-based PLSR modeling for phosphate prediction in Mural Plaster.

3. Results

3.1 Statistical Analysis of Mural Plaster EC Values

The electrical conductivity (EC) values of the mural plaster samples directly reflect variations in salt content within materials of the same composition, thereby exhibiting noticeable variability. Statistical analysis reveals that the EC values range from 2.27 to 4.86 ms·m^{-1}. The mean and standard deviation are 3.55 ± 0.75 ms·m^{-1}, respectively. The first quartile (Q1) and third quartile (Q3) are 2.98 ms·m^{-1} and 4.15 ms·m^{-1}, indicating that 50 % of the samples fall within this interval. Additionally, the coefficient of variation (CV) is 21 %, suggesting a moderate level of relative variability in EC values.

3.2 Analysis of Original Spectral Characteristics of Salt-Containing Samples

The reflectance spectra of salt-bearing mural plaster samples are predominantly influenced by factors such as material composition, salt concentration, and moisture content. Extracting characteristic spectral bands is essential for enabling accurate inversion of salt content. As illustrated in Figure 4, the colored curves represent the average spectral reflectance of the mural plaster samples, while the shaded gray areas denote the standard deviations. Although the reflectance profiles across samples with varying salt concentrations exhibit consistent shapes and trends—indicating a general spectral similarity—distinct variations in absolute reflectance levels are observed, reflecting the influence of salt content on spectral reflectance.

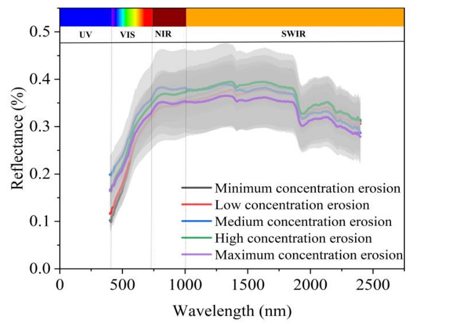

Figure 4 spectral data of mural samples under different conditions

Observations in Figure 4 reveal that in the 400–700 nm range (visible spectrum), reflectance increases sharply with wavelength, resulting in steep spectral slopes. Between 700 and 1800 nm (near-infrared to shortwave infrared), reflectance continues to rise but at a more moderate rate. In contrast, the 2200–2400 nm region demonstrates a generally declining trend, albeit with some fluctuations.

3.3 Analysis of Fractional Order Differentiation (FOD) Results

Fractional order differentiation (FOD) offers a refined approach to hyperspectral data processing by flexibly controlling the differentiation step size, thus achieving an optimal balance between feature enhancement and noise suppression. This is particularly advantageous for high-dimensional hyperspectral data where salient features are difficult to isolate. Following the methodology described in Section 2.3.3 and drawing on the approach of Jie Zhang et al, differentiation orders ranging from 0 to 2 at an interval of 0.1 were applied. The resulting average spectra of mural plaster samples are presented in Figure 5.

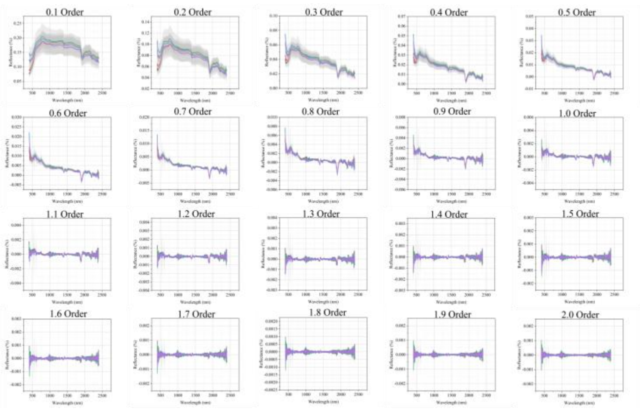

Figure 5 Average fractional-order derivative spectra of Mural Plaster samples. The range of orders spans from 0 to 2, with a step size of 0.1. Colored spectral data represent the average spectra of Mural Plaster samples, while the gray shadow indicates their standard deviation.

The results show that, post-FOD processing, three prominent moisture absorption valleys emerge around 1400 nm, 1900 nm, and 2200 nm—features known to correspond to water absorption characteristics. Although the samples were naturally air-dried after phosphate degradation experiments, the treatments increased sample porosity and surface roughness, enhancing water retention capacity. Moreover, phosphates are hygroscopic under ambient conditions, further elevating sample moisture levels. These water-associated spectral regions may, therefore, contain meaningful indicators of phosphate presence.

As the differentiation order increases, spectral profiles undergo notable transformation. At the 0.5 order, reflectance values oscillate around zero and begin to exhibit negative values across the full wavelength range. By the 0.3 order, reflectance values already fall below 0.1. Beyond the 0.5 order, distinctions among spectral curves initially amplify but then gradually converge into a single trend. After the 1.1 order, changes slow considerably, and spectral contours become increasingly blurred and overlapped—especially beyond the 0.6 order. This suggests that at higher differentiation orders, spectral detail becomes obscured, and inter-curve distinctions diminish. Between orders 1.1 and 2.0, vertical axis values stabilize within ±0.001.

In the context of developing inversion models for phosphate content in mural plaster, FOD proves effective in amplifying spectral differences and enhancing informative features. This phenomenon can be theoretically explained via the Grünwald–Letnikov (G-L) differentiation method. Since reflectance profiles inherently contain broad peaks and troughs, using a sampling step smaller than their widths accentuates differences during computation, thereby highlighting spectral features. However, differentiation inevitably introduces high-frequency noise, especially where reflectance peaks and troughs are closely spaced or have sharp transitions.

Following phosphate erosion experiments at varying concentrations, the samples exhibited notable alterations in salt content, moisture levels, porosity, and surface roughness. Apart from the three water absorption valleys, several distinct reflectance peaks emerge around 400 nm, 870 nm, 1000 nm, 2050 nm, and 2400 nm—with greater clarity at higher differentiation orders. These spectral features are likely linked to the presence of phosphates or organic compounds within the mural plaster matrix. Concurrently, absorption features become increasingly narrow, and distinct material-specific characteristics appear less pronounced at higher orders of FOD.

Notably, in the 700–1300 nm region, reflectance values are generally low but exhibit a rightward shift with increasing concentration, potentially indicating interactions between phosphates and certain mineral or organic components of the mural plaster . This observation underscores the ability of differentiated spectra to reveal information that is not apparent in raw spectral data, such as red-edge positions.

A comparison between first- and second-order derivatives reveals that relying solely on integer-order differentiation may result in substantial information loss. In contrast, fractional-order differentiation strikes a more effective balance between feature enhancement and noise control, making it particularly suitable for the detailed analysis required by hyperspectral datasets.

3.4 Trends in the Correlation Between Fractional Order Differentiation and Salinity

This section examines the correlation between phosphate concentrations in mural plaster and hyperspectral reflectance data, utilizing an adaptive fractional order differentiation (FOD) algorithm based on machine learning. The principal objective is to illustrate the distinct advantages of FOD over traditional integer-order differentiation in processing such spectral data. By identifying the maximum absolute correlation coefficients and their corresponding wavelengths under various differentiation orders, this method demonstrates the enhanced analytical efficiency of FOD, thereby providing crucial support for subsequent data modeling efforts.

Table 3 summarizes the optimal correlations between FOD-processed spectra and phosphate content in the mural plaster, along with their associated wavelengths. At differentiation orders ranging from 0.1 to 0.8, the optimal correlation coefficients are positive, predominantly occurring near 408 nm. Conversely, for orders between 0.9 and 1.7, the highest correlation coefficients are negative, corresponding to wavelengths at 874 nm, 847 nm, and 2064 nm—all situated within the short-wave infrared (SWIR) region. At orders between 1.8 and 2.0, the correlations become positive once more, with the highest positive coefficient observed at order 1.9, corresponding to 2077 nm.

Table 3 Optimal Correlation between the Fractional Order Differential Spectra and Phosphate Content in Mural Plaster, Along with Corresponding Spectral Bands.

Differential order	0.1	0.2	0.3	0.4	0.5	0.6	0.7	0.8	0.9	1
Correlation coefficient	0.509	0.512	0.515	0.518	0.522	0.526	0.526	0.512	-0.527	-0.606
Wavelength (nm)	408	408	408	408	408	408	408	401	874	874
Differential order	1.1	1.2	1.3	1.4	1.5	1.6	1.7	1.8	1.9	2
Correlation coefficient	-0.633	-0.619	-0.579	-0.556	-0.539	-0.544	-0.543	0.549	0.552	0.543
Wavelength (nm)	847	847	874	874	2064	2064	2064	2077	2077	2239

As illustrated in Figure 6, the correlation coefficients between FOD-processed spectra and phosphate concentration vary significantly across different fractional orders. Within the 0.1–0.7 range, the absolute values of the maximum correlation coefficients show minor fluctuations, exhibiting consistent trends across the visible and near-infrared regions. A particularly notable transition from positive to negative correlations is observed in the visible spectrum. Further analysis reveals that phosphate concentrations exhibit heightened sensitivity within the following spectral bands: 400–490 nm, 790–820 nm, 840–890 nm, 1150–1170 nm, 1380–1390 nm, 1465–1480 nm, 1760–1790 nm, 2060–2090 nm, 2190–2210 nm, and 2240–2290 nm. As the differentiation order increases from 0 to 1, the number of spectral bands passing the $p < 0.01$ significance threshold initially decreases, then increases. Notably, the 1.9-order differentiation yields the global maximum positive correlation ($r = 0.552$ at 2077 nm), and identifies six prominent feature wavelengths—2077, 2064, 1470, 402, 1786, and 1712 nm—which align closely with the previously id entified sensitive bands. In contrast, feature bands extracted via integer-order differentiation display lower consistency: the first-order spectrum partially overlaps with key bands (e.g., 874, 848, 854, 2239 nm), while the second-order spectrum demonstrates significant deviation (e.g., 2239, 1180, 1605, 1756, 2063, 1793 nm).

These results indicate that FOD offers heightened sensitivit y and selectivity in capturing phosphate-related spectral features, particularly at the 1.9-order, where it effectively enhances weak absorption features while suppressing spectral noise. This, in tu rn, improves both the robustness and predictive accuracy of sub sequent inversion models. Therefore, the 1.9-order FOD spectru m is preliminarily identified as the optimal order for constructin g hyperspectral inversion models of phosphate concentration in mural plaster. Nevertheless, to ensure model generalizability an d reliability, it remains essential to compare multiple FOD order s and assess their capacity to elucidate the spectral-phosphate co upling mechanisms—thus enabling precise, non-invasive diagn ostics of mural salt damage.

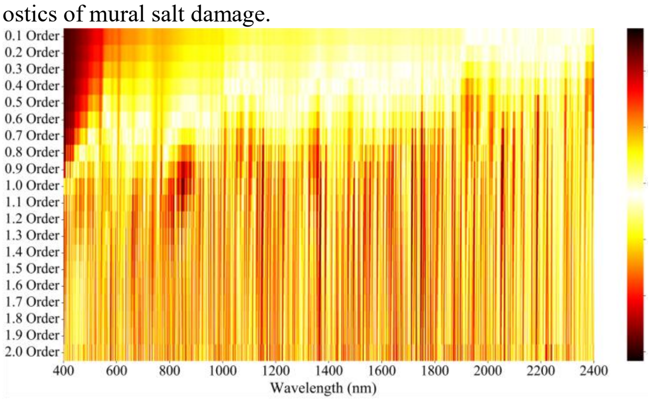

Figure 6 Correlation coefficients between differential spectra at different orders and the phosphate content in Mural Plaster.

3.5 Construction of the Phosphate Inversion Model Based on FOD Spectra

To assess the capability of FOD in predicting phosphate co ncentration in mural plaster, this study adopts the methodology of, analyzing both raw reflectance spectra and FOD spectra rang ing from 0.1 to 2.0 (at 0.1 intervals). Significant spectral bands were selected using correlation-based significance testing and F OD-based feature selection to serve as predictors in the inversio n model.

When evaluating the performance of Partial Least Squares Regression (PLSR) models under varying phosphate concentrati ons and FOD orders (FOD-PLSR), the number of spectral bands used for modeling was determined via significance analysis ($p < 0.01$). Model performance was assessed using MAE, R^2, and RMSE for both calibration and validation datasets, as shown in Table 4.

Table 4 Monitoring Models and Validation Results for Phosphate Content in Mural Plaster.

Order	Number of bands	Calibration Dataset			Validation Dataset		
		MAE_c	R_c^2	$RMSE_c$	MAE_v	R_v^2	$RMSE_v$
0.1	110	0.431	0.509	0.498	0.453	0.485	0.527
0.2	96	0.431	0.511	0.498	0.456	0.475	0.531
0.3	91	0.433	0.511	0.498	0.456	0.454	0.537
0.4	76	0.421	0.496	0.499	0.451	0.471	0.534
0.5	71	0.349	0.638	0.426	0.426	0.557	0.516
0.6	69	0.395	0.629	0.442	0.456	0.549	0.506
0.7	84	0.284	0.739	0.368	0.382	0.561	0.475
0.8	110	0.281	0.752	0.362	0.342	0.676	0.439
0.9	171	0.229	0.820	0.303	0.337	0.714	0.413
1	205	0.167	0.913	0.217	0.323	0.716	0.393
1.1	225	0.134	0.943	0.174	0.320	0.706	0.412
1.2	220	0.103	0.766	0.129	0.304	0.729	0.381
1.3	204	0.121	0.956	0.157	0.321	0.743	0.387
1.4	194	0.111	0.958	0.142	0.303	0.733	0.377
1.5	178	0.159	0.953	0.156	0.363	0.685	0.416
1.6	176	0.174	0.968	0.131	0.404	0.673	0.429
1.7	169	0.248	0.884	0.255	0.426	0.580	0.478
1.8	161	0.191	0.918	0.209	0.382	0.708	0.422
1.9	163	0.078	0.984	0.057	0.312	0.783	0.371
2	162	0.089	0.978	0.109	0.392	0.561	0.467

Table 4 compares model accuracy under integer-order and fractional-order differentiation. Notably, the first-order different iation model exhibits a higher R^2 value than the second-order m odel in the validation set, reaching a maximum of 0.716—highli ghting its superior predictive capability for phosphate content. With increasing differentiation orders, model performance fluct uates. At order 1.9, the model achieves optimal performance, wi th an R^2 of 0.783—outperforming both the integer-order models and the raw spectral model. These results underscore the effica cy of FOD in enhancing data processing, particularly at 1.9-orde r.

Specifically, the 1.9-order FOD model yields an RMSE of 0.057 and MAE of 0.078 in the calibration set, and 0.371 and 0. 312, respectively, in the validation set—demonstrating excellent predictive accuracy and stability.

Experiment result illustrates the optimal phosphate inversi on models based on selected FOD feature bands: (a) first-order, (b) second-order, (c) 1.1-order, and (d) 1.9-order models. Amon g them, the 1.9-order model achieves the best performance in th e calibration set ($R^2 = 0.984$, RMSE = 0.057) and in the validati on set ($R^2 = 0.783$, RMSE = 0.371), affirming its accuracy and r eliability.

In comparison, while the first-order model performs well i n the calibration set ($R^2 = 0.913$), its validation performance dec lines significantly. The second-order model, despite achieving t he highest R^2 in calibration (0.978), suffers the most pronounce d drop in validation ($R^2 = 0.561$), suggesting potential overfittin g. Meanwhile, the 1.1-order model offers a more balanced perfo rmance across both datasets ($R^2 = 0.943$ and 0.706; RMSE = 0.1 74 and 0.412), indicating its potential as a robust alternative. Ov erall, the 1.9-order FOD model is identified as the optimal inver sion model for phosphate monitoring in mural plaster, given its superior accuracy and generalizability.

In summary, the first-order model outperforms the second-order model in both calibration and validation. However, the 1.9 -order FOD model demonstrates the highest prediction accuracy for phosphate content, making it the most suitable choice for hy perspectral inversion in this context.

3.6 Comparison of PLSR Model Performance Using Multi-Feature Selection Algorithms

Table 5, along with Figures 7 and 8, compares the performance of PLSR models built using various feature selection methods in predicting phosphate concentrations in mural plaster. Overall, the LASSO-CC-PLSR (hereafter referred to as LCP) model outperforms those constructed using SiPLS, Random Frog, SPA, and CARS. As the FOD order increases, the predictive capability of the LCP model initially improves, stabilizing after order 1.1. The model reaches peak performance

https://doi.org/10.5194/isprs-archives-XLIX-B2-2026-859-2026 | © Author(s) 2026. CC BY 4.0 License.

at order 1.9 (R^2 = 0.908, MAE = 0.192, RMSE = 0.233). Remarkably, across all differentiation orders, the LCP model consistently achieves the highest accuracy, particularly within the 1.3–1.9 order range.

Table 5. Comparison of Optimal FOD Orders and Predictive Performance Across Feature Selection Methods.

Feature Selection Method	Optimal FOD Order	R^2（Test Set）
CC	1.9	0.783
CARS	1.9	0.870
SiPLS	1.3	0.633
Random Frog	1.9	0.739
SPA	1.4	0.819
LASSO	1.9	0.908

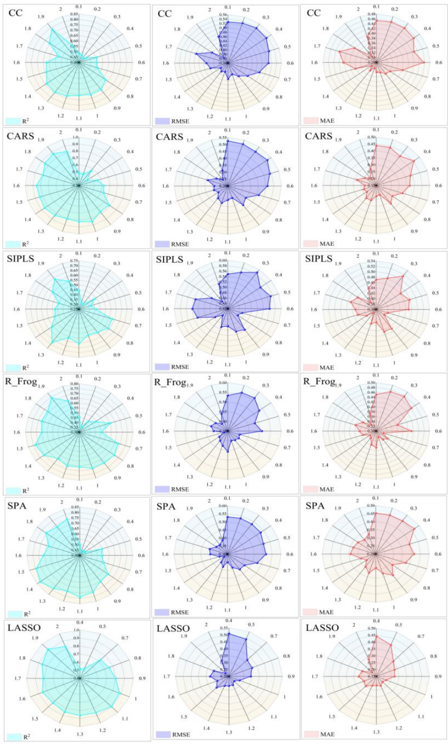

Figure 7. Comparative Analysis of PLSR Models Based on Various FOD Spectra and Feature Selection Methods.

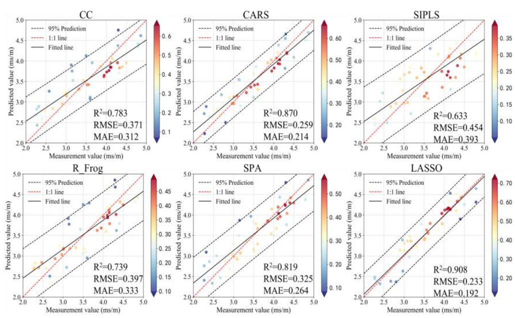

Figure 8. Optimal PLSR Models Constructed Using Different FOD Spectra and Feature Selection Strategies.

In conclusion, the LASSO-based feature selection method significantly enhances model precision, contributing to the high-accuracy, non-contact quantification of phosphate content in mural plaster. This approach exemplifies the efficacy of machine learning-driven adaptive differentiation in hyperspectral analysis.

4. Discussion

Different feature selection algorithms offer distinct advantages, underscoring the necessity of spectral variable screening during model construction. Furthermore, multicollinearity arising from high inter-variable correlation can compromise model performance. Compared with conventional regression methods, Partial Least Squares Regression (PLSR) not only effectively mitigates multicollinearity in high-dimensional spaces but also captures nonlinear coupling relationships, thereby enhancing both explanatory power and predictive accuracy. Thus, the choice of PLSR as the inversion algorithm establishes a robust theoretical and methodological foundation for this study.

Subsequent results reveal that combining PLSR with feature bands selected via both significance testing (correlation coefficient, $p < 0.01$) and LASSO regularization markedly improves the accuracy of phosphate concentration inversion models for the Mural Plaster layer (see Figure 10). This outcome further highlights the pivotal role of machine learning in adaptively identifying sensitive spectral features. However, under certain FOD preprocessing conditions—specifically at orders between 0.1–0.3 and at 0.6—no significant bands were selected. This limitation likely results from the compounded effect of stringent p-value thresholds, the sparsity constraints imposed by LASSO, and the limited sample size. This observation suggests that, in scenarios involving small datasets or low signal-to-noise ratios, it may be necessary to relax the significance threshold or adopt more robust feature selection strategies to prevent the exclusion of potentially informative variables and to ensure optimal model performance.

This study is subject to several limitations. First, although the laboratory-prepared Mural Plaster specimens successfully simulated gradients in porosity and salinity, they cannot fully replicate the complex and dynamic processes of long-term salt migration, crystallization, and dissolution observed in real murals. Future research should incorporate in situ mural testing to validate the stability and applicability of the proposed models. Second, the current investigation focuses on a single salt type, thereby neglecting potential spectral interferences and chemical interactions arising from the coexistence of multiple salts (e.g., sulfates, chlorides) commonly found in mural environments. Subsequent studies should integrate structural characterization techniques such as XRD and FT-IR to construct more comprehensive models accounting for multi-mineral and multi-salt interactions.

Lastly, although PLSR demonstrates strong performance in small-sample scenarios, its linear assumptions may constrain its generalizability when applied to large-scale, heterogeneous hyperspectral imagery. Therefore, future research should explore advanced modeling strategies—such as FOD-enhanced Adaptive Boosting (Adaboost), Extremely Randomized Trees (ERT), and Light Gradient Boosting Machine (LightGBM)—to further refine and identify the most effective predictive frameworks.

5. Conclusions

Through a systematic comparative analysis, this study substantiates the significant enhancement effect achieved by coupling fractional-order differentiation (FOD) spectral transformation with multiple feature selection strategies. The findings demonstrate that integrating FOD with machine learning – based adaptive sensitive band selection markedly improves the predictive accuracy for phosphate content in Mural Plaster. Among the various approaches explored, the 1.9-

order FOD consistently yielded superior predictive performance across the FOD-PLSR, CARS, Random Frog, and LASSO frameworks. In particular, the LASSO-CC-PLSR model achieved the highest accuracy, with a coefficient of determination (R^2) of 0.908 — representing a 15.96 % improvement over the baseline FOD-PLSR model. This study successfully developed a hyperspectral inversion model for phosphate content in Mural Plaster based on the integration of fractional-order differentiation, advanced feature selection methods, and partial least squares regression (PLSR). The resulting model significantly enhances both performance and generalizability, enabling more effective application within the domains of cultural heritage conservation and related hyperspectral remote sensing technologies. Moreover, this approach provides a non-invasive and non-destructive solution for salt damage monitoring, offering a highly efficient and precise alternative to traditional methodologies—many of which are hindered by high costs, inefficiencies, and the potential for physical damage. The proposed model thus represents a substantial advancement in the methodological toolkit available for heritage preservation science.

References

1. Chen L, Lai J, Tan K, Wang X, Chen Y, and Ding J, 2022: Development of a soil heavy metal estimation method based on a spectral index: Combining fractional-order derivative pretreatment and the absorption mechanism. *Science of the Total Environment*, 813, 151882.

2. Fu C-B, Xiong H-G, and Tian A-H, 2019: Study on the effect of fractional derivative on the hyperspectral data of soil organic matter content in arid region. *Journal of Spectroscopy*, 2019. doi.org/10.1155/2019/7159317.

3. Ge X, Ding J, Teng D, Xie B, Zhang X, Wang J, Han L, Bao Q, and Wang J, 2022: Exploring the capability of Gaofen-5 hyperspectral data for assessing soil salinity risks. *International Journal of Applied Earth Observation and Geoinformation*, 112, 102969.

4. Guo Z, Lyu S, and Hou M, 2023: Estimation of the soluble salt concentration in murals based on spectral transformation and feature extraction modelling. *Journal of Applied Spectroscopy*, 90, 1123-1132.

5. Jia P, Zhang J, Liang Y, Zhang S, Jia K, and Zhao X, 2024: The inversion of arid-coastal cultivated soil salinity using explainable machine learning and Sentinel-2. *Ecological Indicators*, 166, 112364.

6. Li X, Yang H, Chen C, Zhao G, and Ni J, 2024: Deterioration identification of stone cultural heritage based on hyperspectral image texture features. *Journal of Cultural Heritage*, 69, 57-66.

7. Małysiak A, Orda S, and Drzazga M, 2021: Influence of Supersaturation, Temperature and Rotational Speed on Induction Time of Calcium Sulfate Crystallization. *Crystals*, 11, 1236. doi.org/10.3390/cryst11101236.

8. Mashimbye Z, Cho M, Nell J, De Clercq W, Van Niekerk A, and Turner D, 2012: Model-based integrated methods for quantitative estimation of soil salinity from hyperspectral remote sensing data: A case study of selected South African soils. *Pedosphere*, 22, 640-649. doi.org/10.1016/S1002-0160(12)60049-6.

9. Ren Y and Liu F, 2024a: A Novel Hyperspectral Salt Assessment Model for Weathering in Architectural Ruins. *ISPRS Annals of the Photogrammetry, Remote Sensing and Spatial Information Sciences*, 10, 201-208.

10. Ren Y and Liu F, 2024b: The spectral inversion model for electrical conductivity in mural plaster following phosphate erosion based on fractional order differentiation and novel spectral indices. *Heritage Science*, 12, 286.

11. Ren Y and Liu F, 2024c: A model for inversion of hyperspectral characteristics of phosphate content in mural plaster based on fractional-order differential algorithm. *Scientific Reports*, 14, 17898.

12. Ren Y and Liu F, 2025: Investigative experiment on in-situ low-temperature crystallization induction time measurement for Dunhuang Murals, considering porosity factors. *npj Heritage Science*, 13, 88.

13. Sansupa C, Suphaphimol N, Nonthijun P, Ronsuek T, Yimklan S, Semakul N, Khrueraya T, Suwannarach N, Purahong W, and Disayathanoowat T, 2023: Life on the wall: the diversity and activity of microbes on 13th–century AD. Lan Na mural painting. *Frontiers in Microbiology*, 14, 1220901.

14. Song G, Wang Q, and Jin J, 2023: Fractional-order derivative spectral transformations improved partial least squares regression estimation of photosynthetic capacity from hyperspectral reflectance. *IEEE Transactions on Geoscience and Remote Sensing*, 61, 1-10.

15. Sousa J V d C, Kucche K D, and De Oliveira E C, 2019: Stability of ψ-Hilfer impulsive fractional differential equations. *Applied Mathematics Letters*, 88, 73-80. doi.org/10.1016/j.aml.2018.08.013.

16. Wang X, Wang J, Wang J, and Tang Y, 2023: ANALYSIS ON THE DAMAGE AND WEATHERING CAUSE OF ARCHITECTURAL HERITAGE ALONG THE MARITIME SILK ROAD: A CASE STUDY OF MINLEDOU WHARF. *International Journal of Conservation Science*, 14, 469-480.

17. Wang X, Zhang F, Ding J, Kung H-t, Latif A, and Johnson V C, 2018: Estimation of soil salt content (SSC) in the Ebinur Lake Wetland National Nature Reserve (ELWNNR), Northwest China, based on a Bootstrap-BP neural network model and optimal spectral indices. *Science of the Total Environment*, 615, 918-930.

18. Zhang Y, Cui D, Liu S, Li B, and Guo H, 2025: Types and sources of salts causing exfoliation and efflorescence in stone relics at Yongling Mausoleum. *npj Heritage Science*, 13, 61.

19. Zhouqian G, Shuqiang L, and Miaole H, 2023: Inversion of salt content in simulated mural based on Hyperspectral mural salt index. *Spectroscopy and Spectral Analysis*, 43, 3272-3279. doi.org/10. 3964/j.issn.1000-0593 (2023)10-3272-08.